# Field validation of a physically-based model for bioretention systems

Jérémie Bonneau [1,2], Gislain Lipeme Kouyi [1], Laurent Lassabatere [4], Tim D. Fletcher [3]

Affiliation

[1] Univ Lyon, INSA Lyon, DEEP, EA7429, 69621 Villeurbanne, France

[2] INRAE, RiverLy, 5 Rue de la Doua, CS 20244, 69625, Villeurbanne, France

[3] School of Ecosystem and Forest Sciences, University of Melbourne, Burnley, Australia

[4] Univ. Lyon, Univ. Claude Bernard Lyon 1, CNRS, ENTPE, UMR5023 LEHNA, F-69518, Vaulx-en-Velin, France

Corresponding author : Jérémie Bonneau, jeremie.bonneau@inrae.fr;
jeremie.bonneau@gmail.com;
INRAE, RiverLy, 5 Rue de la Doua, CS 20244, 69625, Villeurbanne, France

*(From Introduction to Conclusions - 5457 words - 29500 characters)*

**Abstract**

Bioretention systems are increasingly used worldwide to mitigate the impacts of urban stormwater runoff on the water cycle. Being able to accurately model physical processes occurring within these systems is critical to their design and to being able to predict their performance. Most popular urban hydrological models must now integrate a low impact development (LID) toolbox to keep up with current practices. We aimed to develop and test a generic model of bioretention systems that can serve as a targeted compromise between oversimplification without any physical basis, on the one hand, and physical soundness requiring a large number of parameters for calibration, on the other. The model accounts for evapotranspiration, overflow, infiltration into the filter (single permeability behavior), exfiltration to surrounding soils, along with underdrain discharge. The model was tested against field data from a monitored bioretention basin in Melbourne, Australia. Based on 22 rainfall events, results showed that the simulated underdrain outflow rates and their temporal dynamic were well replicated (for 20 rainfall events, median NSE = 0.74, median PBIAS = -22%, median RMSE = 0.48 l/s). Despite good performance for outflow rates, there was a discrepancy observed in magnitude between simulated and measured water levels within the bioretention basin. The model therefore seems a useful first step towards the design of a user-friendly model for assessing both performance and impact of bioretention basins for catchment-scale flow regime management.

**Key words**: Bioretention models, LID toolbox, WSUD, stormwater

**Highlights**:

- We developed a hydrologic model for bioretention basins for modeling outflow rates.
- The model was able to replicate piped outflows from a real case study with two parameters needed for calibration.
- The accurate modeling of water level dynamics within the bioretention filter requires additional soil physical parameters and was not well replicated.

**Graphical abstract**

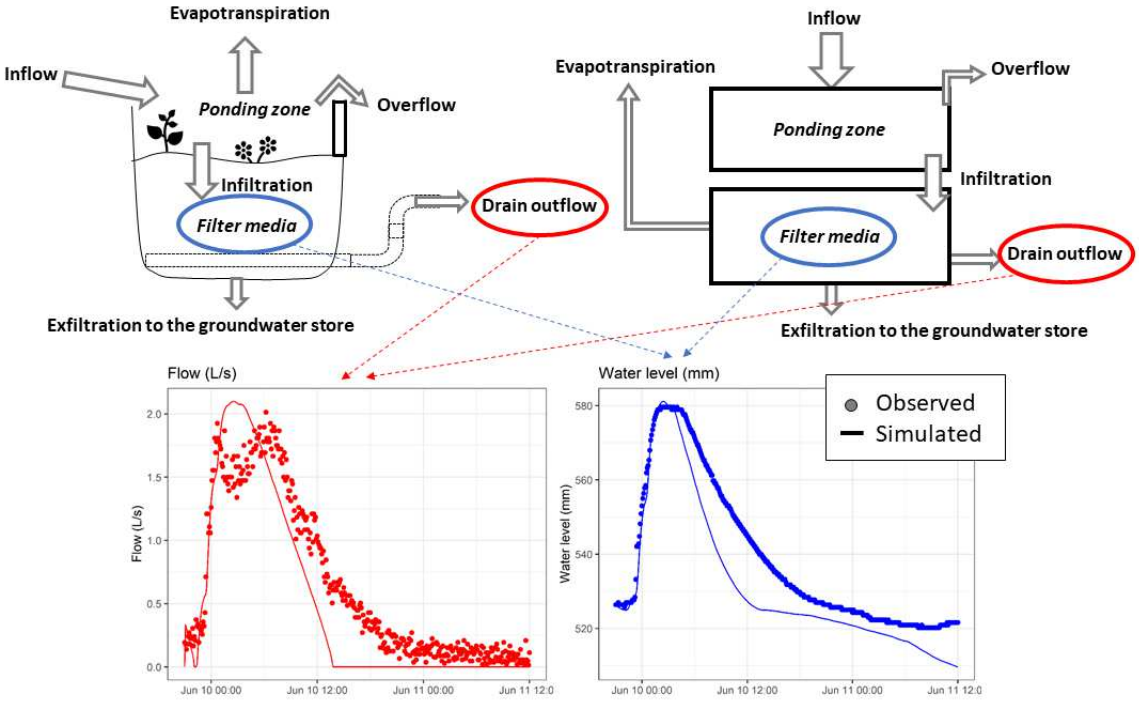

# 1. Introduction

To mitigate the impacts of urbanization on the flow regimes and water quality of water bodies (Walsh et al., 2012), bioretention basins are increasingly used as part of a suite of stormwater control measures (SCMs). Bioretention basins are landscaped depressions filled with sand and gravel, often vegetated, that are designed to receive urban runoff (from roofs, roads, etc.). They provide storage and allow urban runoff to be released to the atmosphere by evapotranspiration and infiltrated in native soils rather than discharged in piped networks to urban streams or other receiving waters. As such, bioretention basins are extremely efficient at reducing urban runoff peak flows, stormwater volumes and pollutants loads (Liu et al., 2014; Roy-Poirier et al., 2010). Their application aims to restore lost fluxes of the water balance (evapotranspiration, infiltration) and to reduce stormwater runoff caused by creation of impervious areas and hydraulically-efficient drainage systems (Burns et al., 2012). Modelling the performance of bioretention basins is, however, a challenge, as physical mechanisms involved in these systems are complex. These requirements can often preclude their use by decision-makers, designers and practitioners, meaning that there is a need for models which can be simply but reliably calibrated using relatively easy-to-collect monitoring data. A model which is physically-based, yet easy to calibrate, could be attractive for urban water management practitioners in current and future cities.

A wide range of tools exist to model Low Impact Development (LID) structures (Elliott and Trowsdale, 2007). The popular SWMM model includes a very flexible landscape-scale infiltration module, offering a choice of Hortonian, Green-Ampt or Curve-Number infiltration (Rossman, Lewis A., 2010; Rossman, Lewis A, 2010). The LID module in SWMM is based on

88 the Green-Ampt infiltration from the surface into the filter media, followed by Darcy's flow
89 through the porous media below, with subsequent infiltration to groundwater assumed to
90 be constant. To model retention in green roofs, Kasmin et al. (2010) present a conceptual
91 process-based model, where the soil is described as a store with different soil moisture
92 thresholds that drive hydrological processes (e.g. runoff produced when soil moisture is
93 higher than field capacity). DRAINMOD is used extensively to model bioretention systems:
94 infiltration is modeled with the Green-Ampt equation (Skaggs, 1980, 1985) and requires the
95 user to specify the soil-water characteristic curve and saturated hydraulic conductivity
96 (Brown et al., 2013). DRAINMOD was recently adapted to the urban case (Lisenbee et al.,
97 2020). Drainage is modeled with the Hooghoudt's equation, taking into account lateral
98 hydraulic conductivity and properties of the underdrain (particularly spacing and radius). In
99 Australia, MUSIC is the industry standard to model bioretention basins and other
100 Stormwater Control Measures (eWater, 2014, 2020). Infiltration within bioretention basins is
101 described in MUSIC by Darcy's equation, accounting for impacts of soil texture and moisture,
102 with infiltration calculated from both the base and sides, while underdrain flow is calculated
103 from Darcy's flow through the porous media, again accounting for texture and degree of
104 saturation. Richards' equation, that combines mass conservation and Darcy's equation
105 (Richards, 1931; van Genuchten, 1980), was used to model flow in bioretention cells to
106 predict peak flow and volume reduction by He and Davis (2011). Other models used the
107 Green-Ampt equations, e.g. Gülbaz and Kazezyılmaz-Alhan (2017).
108
109 In general terms, bioretention models may be separated in two groups. The first group is
110 made up of models that have no extensive physical basis and are mostly designed
111 statistically for a given experimental site, thus requiring a low number of parameters to

implement. However, these models are often case-specific, being difficult to extrapolate to other sites and having limited predictive capabilities. Conversely, the second group is composed of more complex models, that are based on the modeling of physical processes, and usually require significant effort for calibration (Alamdari and Sample, 2019) or access to specific soil parameters which are complicated to estimate (such as the soil water retention curve or the unsaturated hydraulic conductivity). There is thus a need for a third option: models that are simple to calibrate while offering a satisfying level of consistency with regards to the physics of water infiltration in the bioretention systems, the use of more sophisticated models not systematically improving modelling results, since more parameters are needed, and calibration becomes more difficult (Mourad et al., 2005) and thus less likely to be undertaken by decision-makers and system designers.

The aim of this study was therefore to develop and test a simplified, physically-based model requiring low effort for calibration and capturing the hydraulic dynamic of bioretention systems. We report the development and testing of a physically-based hydrologic model against data obtained from a monitored bioretention basin (Wicks Reserve Bioretention system). The modelling approach describes the whole bioretention system as a series of reservoirs storing and exchanging water fluxes. The approach includes consideration of mass conservation (continuity equation), Darcy's equation for the implementation of infiltration fluxes into the system and the soil below, orifice equation for the underdrain, with the computation of evapotranspiration, allowing the prediction of exchanges between the reservoirs, and thus the water level in the filter (body of the bioretention system) and the outflow rates. Therefore, we present a new model that explicitly accounts for physical processes (soil water storage, vertical gravity-driven infiltration, exfiltration, respect of mass

136 balance) under unsteady flow conditions, to predict the outflow performance of
137 bioretention systems. A key objective was to provide explicit and simplified formulation of
138 existing modelling approaches and equations in order to create a physically-based model.
139

# 2. Methods

## *2.1. Model development*

The model is a physically-based representation of bioretention basins, based on reservoirs or storages in series, accounting for the water balance between storages and water fluxes between storages (Figure 1). All equations presented below were discretised using a first order, explicit numerical scheme, considering a fixed 6 minutes timestep, to fit with observed data. The complete algorithm and computation code (R scripts) are available as Supplementary material and the dataset used is publicly shared on the platform Zenodo (Bonneau et al. (2021) http://doi.org/10.5281/zenodo.4717453).

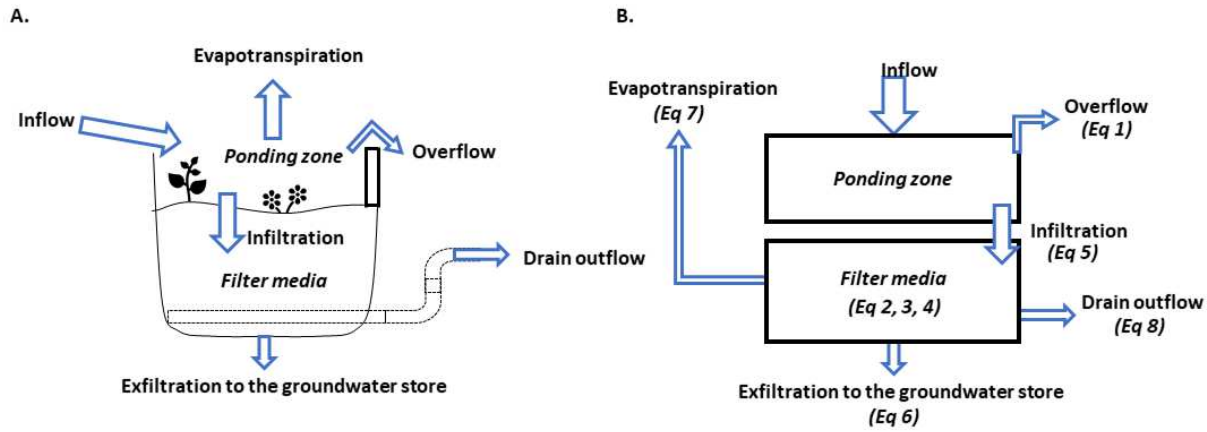


*Figure 1: Conceptual representation of the model*

*First reservoir: the ponding zone*

The first reservoir corresponds to the ponding zone or the surface storage area. It is assumed to be a rectangular empty box (Figure 1). It receives the entering water fluxes that are routed to the bio-infiltration system (Inflow). The inflow hydrograph leads to water level in the ponding zone which acts as the upstream boundary condition.

This reservoir has a maximum capacity. When the water level exceeds a given threshold, an overflow pit or weir diverts excess water out of the surface storage. In the model, a threshold level is set by the user so that when the water level in the surface storage is greater than this threshold, water is diverted producing an overflow rate computed by mass balance consideration (Eq. 1).

$$if\ h_{pond} < h_{weir}, Q_{ovf} = 0$$

$$Otherwise, Q_{ovf} = Q_{in} - Q_{inf} \text{ (Eq. 1)}$$

Where $h_{pond}$is the water level in the surface storage, $h_{weir}$ the height of the overflow weir, $Q_{ovf}$ the overflow rate, $Q_{in}$ the inflow entering the ponding zone, $Q_{inf}$ flux of water infiltrating into the filter below.

*Second reservoir: the filter of the bioretention system:*

The second reservoir represents the filter that constitutes the main body of the bioretention system (Figure 1). The filter receives the infiltration flux from the surface storage, and loses water due to evapotranspiration, infiltration into the subsoils and to the outflow pipe collected by an underdrain.

The infiltration from the ponding zone into the filter was modelled using a Darcian approach, which is simple and commonly used to compute water fluxes in porous media (Bear, 1972). The van Genuchten (1980) and Mualem (1976) models are among the most widely used for the water retention and the unsaturated hydraulic conductivity functions and read as follows (Eq. 2):

179 $$S_e = \frac{\theta - \theta_r}{\theta_s - \theta_r} = \left(1 + (\alpha h)^{1/(1-m)}\right)^{-m} (Eq.\,2a)$$

180 $$K(S_e) = K_s S_e{}^{\tau} \left[1 - \left(1 - (S_e)^{\frac{1}{m}}\right)^{m}\right]^2 (Eq.\,2b)$$

181 Where $S_e$ is the saturation degree, $\theta$ the volumetric water content, $\theta_s$ the saturated
182 volumetric water content and $\theta_r$ is the residual water content, α a fitting parameter related
183 to water pressure head; *m* (m = 0.5 for coarse soils, with the sand/gravels used for the filter
184 and drainage layer) and τ (τ = 0.5, default values for tortuosity) are shape parameters, $K$ is
185 the unsaturated hydraulic conductivity (m $s^{-1}$), $K_s$ the saturated hydraulic conductivity (m $s^{-1}$).

186

187 To diminish the number of parameters in the model, some simplifications were proposed, as
188 described below. The behaviour of the filter media was simplified by considering that it
189 behaves like coarse material with a stepwise water retention function, as mostly considered
190 for coarse media (Lassabatere et al., 2021). In that case, the water profile takes the shape of
191 a step function, with saturated conditions below the height of water and dry conditions
192 above. Eq. 2a is then replaced with a stepwise function and the parameter α is no longer
193 needed. Considering a stepwise profile, the average saturation degree can be linked to the
194 height of water in the filter media (Eq. 3):

195 $$\bar{Se} = \frac{F}{F_{max}} \ (Eq.\,3)$$

196 Where $\bar{Se}$ is the average saturation degree at any time, *F* the height of water in the filter,
197 i.e., the positive hydraulic head from the bottom of the filter, and $F_{max}$ represents the total
198 thickness of the filter layer. For simplicity, the term 'filter layer' is considered hereafter to

include the drainage layer. The hydraulic conductivity was then derived by applying the Mualem model (Eq. 2b) to the average saturation-degree, leading to the following expression for the unsaturated hydraulic conductivity:

$$K\left(\frac{F_{i-1}}{F_{max}}\right) = Ks\left(\frac{F_{i-1}}{F_{max}}\right)^{\tau}\left[1-\left(1-\left(\frac{F_{i-1}}{F_{max}}\right)^{\frac{1}{m}}\right)^{m}\right]^{2} \quad (Eq.4)$$

We considered at any time *i*, the previous saturation degree $\overline{Se}_{i-1} = \frac{F_{i-1}}{F_{max}}$. Note that the application of Darcy's equation allowed the quantification of the infiltrating flux rate by multiplying the unsaturated hydraulic conductivity (Eq. 4) with the hydraulic gradient. However, during the considered time step, no more than the volume of water available in the surface storage can infiltrate. In addition, no more than the volume available in the filter can be filled by the infiltrating water. These two conditions impose two limitations (Eq 5b. and 5c.). Finally, the infiltration rate into the filter media was obtained using the following equation (Eq. 5):

$$Q_{inf,i} = min\begin{pmatrix} \frac{F_{max} - F_{i-1} + h_{pond,_{i-1}}}{F_{max}} K\left(\frac{F_{i-1}}{F_{max}}\right) A & (Eq.5.a.) \\ (F_{max} - F_{i-1})\frac{A}{\Delta t}\eta_f + \sum Q_{outs,i} & (Eq.5.b.) \\ h_{pond,_{i-1}} \times \frac{A}{\Delta t} + Q_{in,i} & (Eq.5.c.) \end{pmatrix}$$

where *A* is the mean area of the bottom of the ponding store, $\Delta t$ is the time step, $\eta_f$ is the mean porosity of the filter layer, $Q_{in,i}$ is the observed inlet flow rate at the time step *i* and $\sum Q_{outs,i}$the sum of all outflows from the filter media at the time step *i* (in this case underdrain outflow, evapotranspiration and exfiltration to the native soil). Eq 5.a. in the function "min" corresponds to the application of Darcy's law, assuming the hydraulic conductivity detailed in equation (Eq. 4). Eq 5.b.and Eq 5.c were set to respect the mass balance of the system. Eq 5.b. enables computation of infiltration rate when the storage

capacity within the filter limits the amount of water that could infiltrate (typically at the end of an event). Eq 5.c. enables computation of infiltration rates when all the ponded water can infiltrate during the time step i, typically at the start of an event with dry initial conditions.

The remaining fluxes were computed as follows. The exfiltration of water by infiltration into the surrounding native soil was computed as a function of its hydraulic conductivity and the wetted surface of the filter:

$$Q_{exf} = K_{s\,inf}\ S_{wet}\ (Eq.6)$$

Where $K_{s\,inf}$ is the saturated hydraulic conductivity of the surrounding soil and $S_{wet}$ is the wetted area of the filter storage, i.e., the contact surface between water and the surrounding soil. The flow in the native soil was then considered gravity-driven without capillarity-driven infiltration.

The evapotranspiration resulting from plant root systems developed in the filter was calculated from potential evapotranspiration (thus assuming a crop factor of 1.0) and modulated with a linear function between the wilting point and field capacity (Eq. 7) (Francés, 2008; Van der Lee and Gehrels, 1990):

$$if\ \theta < \theta_w, Q_{etr} = 0$$

$$if\ \theta_w < \theta < \theta_{fc}, Q_{etr} = \frac{\theta - \theta_w}{\theta_{fc} - \theta_w} Q_{etp}$$

$$if\ \theta > \theta_{fc}, Q_{etr} = Q_{etp} \quad (Eq.7)$$

Where $\theta_w$ and $\theta_{fc}$ are the wilting point and the field capacity, respectively, taken as usual valued for sandy soils (FAWB, 2015), $Q_{etr}$ is the real evapotranspiration rate and $Q_{etp}$ the potential evapotranspiration rate, sourced from a nearby meteorological station of the

242 Australian Bureau of Meteorology (Station 086266, Lat -37.87, Lon 145.35, calculated with
243 the Morton method, from the SILO database)(BoM, 2021; SILO, 2020).
244
245 Lastly, the outflow collected by the underdrain was computed with an orifice equation (thus
246 assuming the pipe itself does not limit flow), according to Eq. (8):
247 $$Q_{out,i} = C_{out}\sqrt{2gH}\ (Eq\ 8)$$
248 Where $C_{out}$ is an orifice coefficient to be calibrated, *g* the acceleration due to gravity and *H*
249 the difference between water level in the filter and the level of the underdrain orifice (Figure
250 1).
251

## 2.2. *Case study*

### 2.2.1. Bioretention basin and catchment description

Wicks Reserve Bioretention Basin (hereafter referred to as "the basin") is located in the eastern suburbs of Melbourne, Australia (Bonneau et al., 2018). Stormwater enters the basin by two stormwater pipes draining a combined 5 ha of impervious areas (estimated using geographic information provided by the local municipality, and corroborated with rainfall-runoff data) connected to a conventional, separate stormwater network, in a 33-ha residential catchment. The catchment responds to rainfall quickly, with flow in pipes observed around 30-45 minutes after rainfall. At the location of the basin, groundwater is deeper than 4 m below the surface. The basin is 1800 $m^2$ in area, and on average 0.8 m deep (350 mm loamy sand-based filtration media overlaying 300 mm of 20 mm scoria gravel, with three 50 mm deep transition layers - medium-fine sand, coarse sand and 7-10 mm gravel - in between them). There is a slotted underdrain at the base of the infiltration system, which discharges through an elevated orifice in a discharge pit. The underdrain is connected back to the stormwater network ("Outlet"). The orifice is elevated by 500 mm from the invert of the basin, meaning that the bottom 500 mm acts as a 'saturated zone', with discharge below this depth occurring only through infiltration (Figure 2). Above this depth both infiltration and underdrain discharge may occur. The hydraulic conductivity of the surrounding native soil was measured by fitting recession events (water level drop in the filter) and confirmed with in-situ rising stage slug test with the Bouwer Rice method and found to be quite low, around 1 mm $hour^{-1}$ or 2.8 x $10^{-7}$ m $s^{-1}$. Large flows (> 200 L/s) are diverted from the basin into a bypass pipe via a weir ("Bypass pipe") immediately upstream of the basin, to ensure excessively large flows do not damage the basin surface or vegetation.

The runoff from the basin's catchment is conveyed in two stormwater drains (Figure 2) and the inlet flow passes through a Gross Pollutant Trap (GPT) and a sedimentation pond before flowing onto the filter area of the bioretention basin. Indeed, the presence of the pond and the GPT delays inflow getting into the bioretention basin. In the model, we inserted a linear reservoir with a lag time of 15 min (assessed thanks to site observations and knowledge of the system) to account for the delay and the transformation of the inflow hydrograph due to GPT and sedimentation pond.

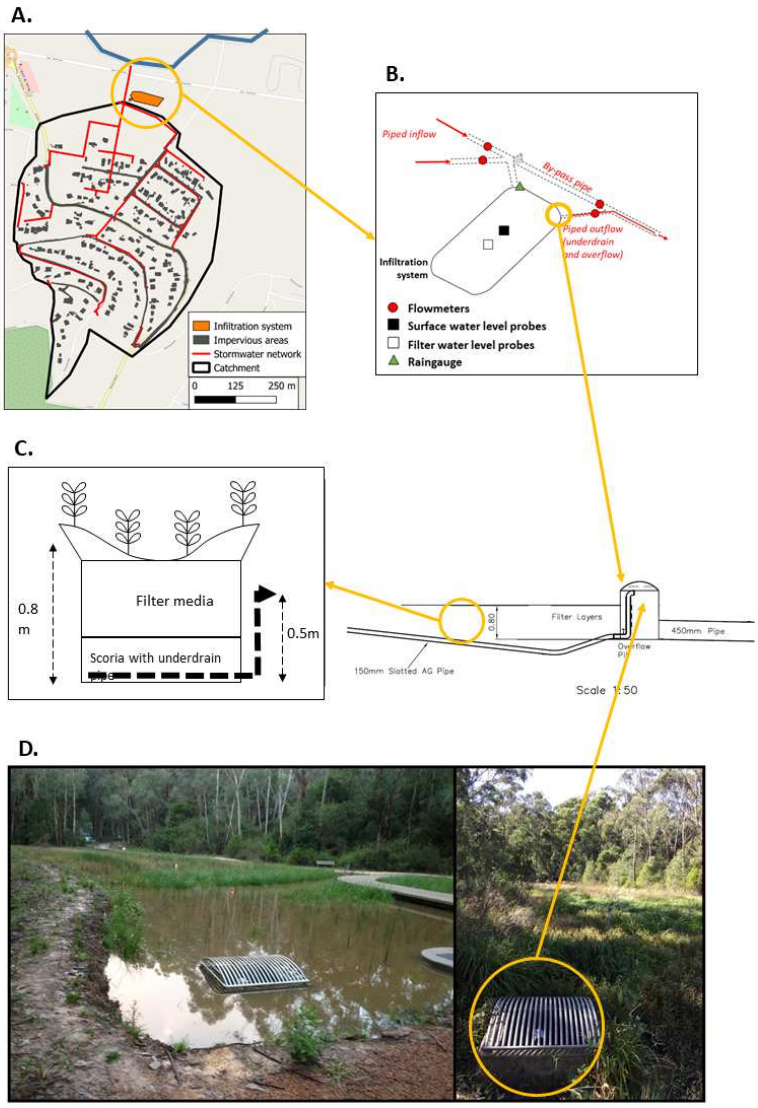


*Figure 2: A: Map of the catchment feeding the bioretention basin (source: Bonneau et al., 2020) B: Monitoring system. C: Transect of the filter of Wicks Reserve Bioretention basin D: Photos of the basin (sourcre: Bonneau et al., 2020).*

### 2.2.2. Monitoring and data presentation

The basin was monitored using four Sigma 950 flowmeters, one in each inlet pipe, and one in each of the bypass and outlet pipes (Figure 2), so that inflow to the basin and outflow through the underdrain could be measured and compared. Flow velocity was measured with a Doppler probe and water level with a pressure diaphragm. Small weirs were built in pipes to ensure the probes remained submerged. The flowmeters were manually calibrated: manual flow measurements were performed regularly for high and low flows to obtain the best relationship between the actual flow and the probe values (flow rate, level, velocity). Data were collected from March 2013 to September 2016 (Bonneau et al., 2020). In addition, water levels in the ponding zone and within the filter were also monitored, using Odyssey capacitance probes. An Odyssey rain-gauge monitored rainfall using a 0.2 mm tipping bucket. The basin was monitored from July 2013 to December 2016. Flow rate, water level and rainfall were recorded at a 6 minutes timestep. In total, 22 rainfall events were selected over the period to be used for the calibration (2 events) and validation (20 events) of the model, ranging from 1 mm to 46 mm, with a median rainfall total of 7.7 mm.

### 2.2.3. Calibration and performance indicators

The objective of the model was to replicate the measured outflows, since this is the variable of most interest for stormwater managers. The goodness of fit between observed and simulated outflows was assessed by calculating the Nash Sutcliffe Efficiency (NSE; Eq. 9, (Nash and Sutcliffe, 1970)).

$$NSE = 1 - \frac{\sum_{i=1}^{N}\left(X_i^{obs} - X_i^{sim}\right)^2}{\sum_{i=1}^{N}\left(X_i^{obs} - \overline{X_i^{obs}}\right)^2} \quad (Eq. 9)$$

With $X_i^{obs}$ the observed outflow value, $\overline{X_i^{obs}}$ the mean of observed value, $X_i^{sim}$ the simulated value, $N$ the number of timesteps per event.

For calibration, the model was run for thousands of combinations of parameters $K_s$ and $C_{out}$ (varied across their physically plausible range: $K_s$ from $10^{-6}$ to 0.1 m/s, $C_{out}$ between 0 and 0.1) for the 2 rainfall events selected for calibration, with respective rainfall totals of 2 mm of rainfall, and 15 mm of rainfall, to cover the range of observed rainfall events. Parameters were adjusted to predict outflows, but the evolution of water levels was also checked to assess how well the model reflected the hydraulic gradient dynamics in the filter. Calibrated parameters $K_s$ and $C_{out}$ were obtained by maximizing the average of $NSE_Q$ for flows for both events.

*Table 1: numerical values of parameters used in the model (bold values refer to the calibrated parameters).*

| **Parameters** | **Value** |
|---|---|
| Filter depth (m) | 0.8 |
| Area of the ponding zone ($m^2$) | 900 |
| Area of the filter ($m^2$) | 1800 |
| Filter porosity | 0.4 |
| Wilting point $\theta_w$ | 0.1 |
| Field capacity $\theta_{fc}$ | 0.2 |
| Surrounding soil hydraulic conductivity (m/s) | 2.8 $e^{-7}$ |
| Shape parameter *m* | 0.5 |
| Tortuosity $\tau$ | 0.5 |
| **Saturated filter media hydraulic conductivity $K_s$ (m/s)** | **$5.10^{-4}$** |

| Orifice coefficient $C_{out}$ | $2\ 10^{-3}$ |
|---|---|

For both calibration events, the saturated hydraulic conductivity of the filter $K_s$ had less impact than the orifice coefficient parameter $C_{out}$. Nash Sutcliffe coefficients of efficiency were positive only for a certain range of tested values (Figure 3). The parameter $K_s$ reached a threshold around $3.10^{-4}$ m $s^{-1}$, from which it had very little impact on the performance of the model, and was fixed to $5.10^{-4}$ m $s^{-1}$. The parameter $C_{out}$, reached 'optimum' values 1.2 x $10^{-3}$ for the first calibration event and 2.5 x $10^{-3}$ for the second calibration event (Figure 3). Average value with $C_{out}$ = 2 x $10^{-3}$ as an average of both previous $C_{out}$ values was taken as the final calibrated value for $C_{out}$ (Table 1).

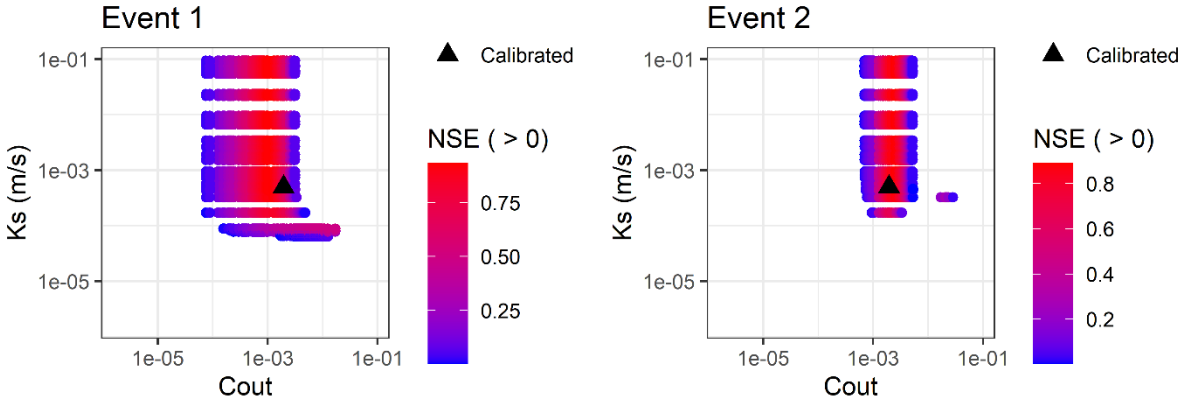


*Figure 3: Evolution of the Nash Sutcliffe Efficiency between observed and simulated outflows for the two calibration events.*

The model was then tested and validated with these parameters against 20 monitored rainfall events, with two additional indicators calculated (Ahmadisharaf et al., 2019; Moriasi et al., 2015): percent bias (PBIAS; Eq 10) and the root mean square error (RMSE, Eq. 11), in order to validate the performance of the model.

$$PBIAS = \frac{\sum_{i=1}^{N}\left(X_i^{sim} - X_i^{obs}\right)}{\sum_{i=1}^{N} X_i^{obs}} \text{ (Eq. 10)} \quad RMSE = \sqrt{\frac{\sum_{i=1}^{N}\left(X_i^{obs} - X_i^{sim}\right)^2}{N}} \text{ (Eq. 11)}$$

With $X_i^{obs}$ the observed outflow value, $\overline{X_i^{obs}}$ the mean of observed value, $X_i^{sim}$ the simulated value, $N$ the number of timesteps per event.

# 3. Results and Discussion

*Validation over 20 rainfall events*

The performance of the model tested over 20 rainfall events (excluding the two calibration events) was satisfying (Figures 4 and 5), with a mean NSE of 0.53, a median NSE of 0.75 and a median RMSE of 0.48 l/s. The model tended to underestimate fluxes, with a median PBIAS of - 22% (Figure 5). Overall, the proposed model was able to well replicate outflows of the basin for most rainfall events (Moriasi et al., 2015). However, the model was not able to replicate water level dynamics in the filter (Mean and median NSE < 0). The water level dynamics in the filter were not broadly well simulated (Figure 6). To better capture observed water levels, additional soil hydrodynamic parameters would likely be required, allowing a better simulation of the complexity of infiltration behavior (e.g., capillarity effects, relationship between water content and hydraulic head, potential preferential flows or air entrapment, etc.), but such information is not always easily available to end-users (Fournel et al., 2013). The approach presented is a compromise between model parsimony and performance, between being able to replicate observed water levels (arguably less important than replicating observed outflows) and further complicating the model and its calibration in practice. Flow data is indeed of the most interest in terms of impacts on water quality and flow regimes of receiving waters (DeBusk et al., 2011). Poor replication of water levels within the filter media possibly indicated oversimplification of geometry of the basin and water infiltration, along with redistribution within the filter.

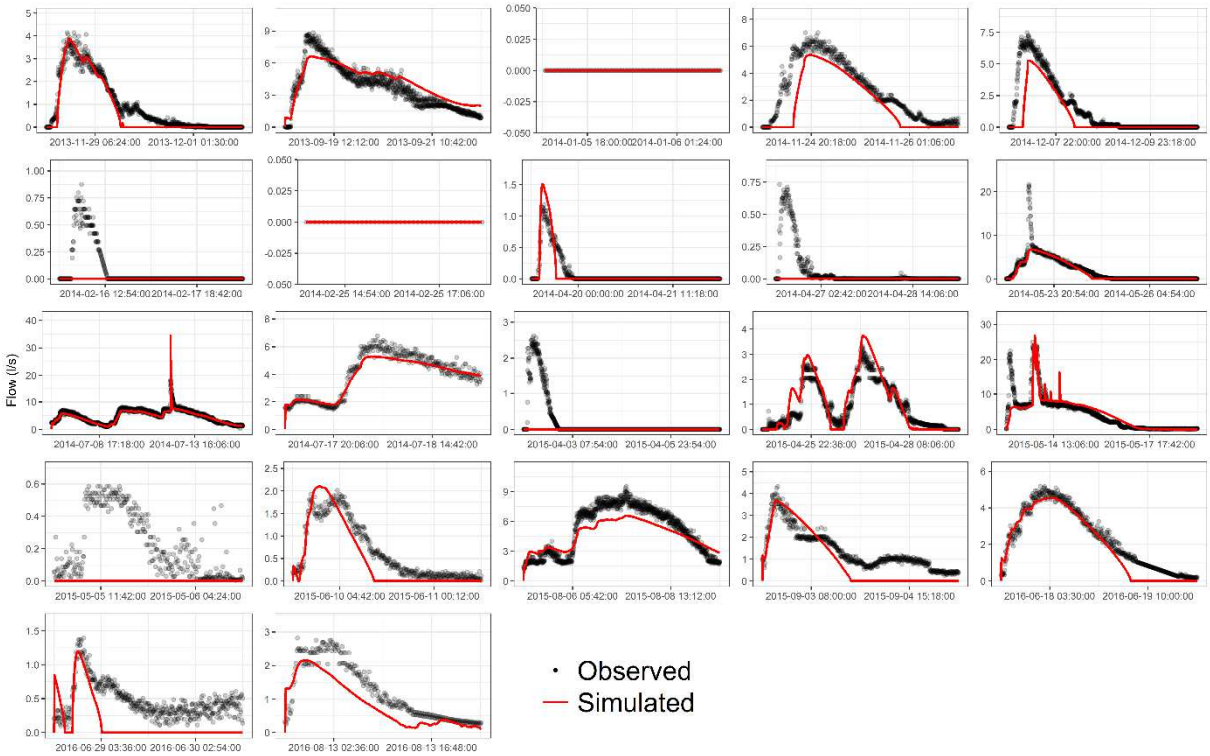


*Figure 4: Observed outflow hydrographs (black line with points = measured; red line = simulated with the proposed model)*

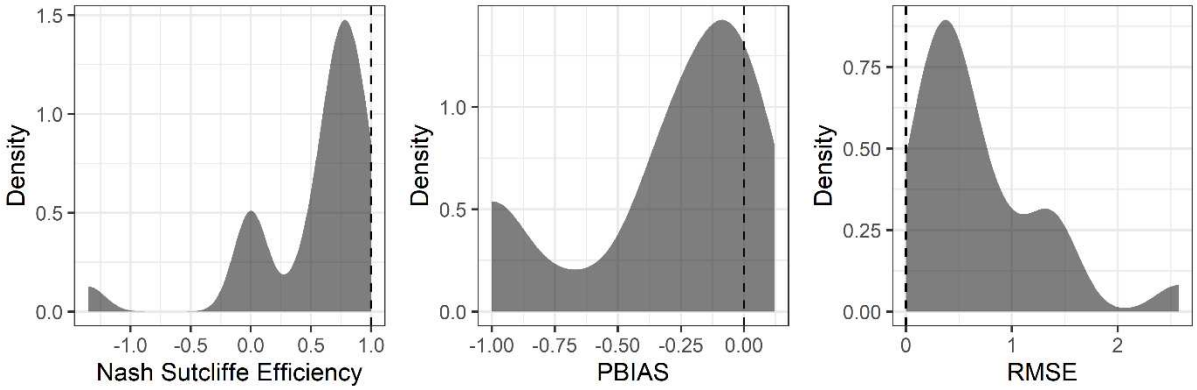


*Figure 5: Distribution of the Nash Sutcliffe efficiencies, PBIAS and RMSE for all the rainfall events.*

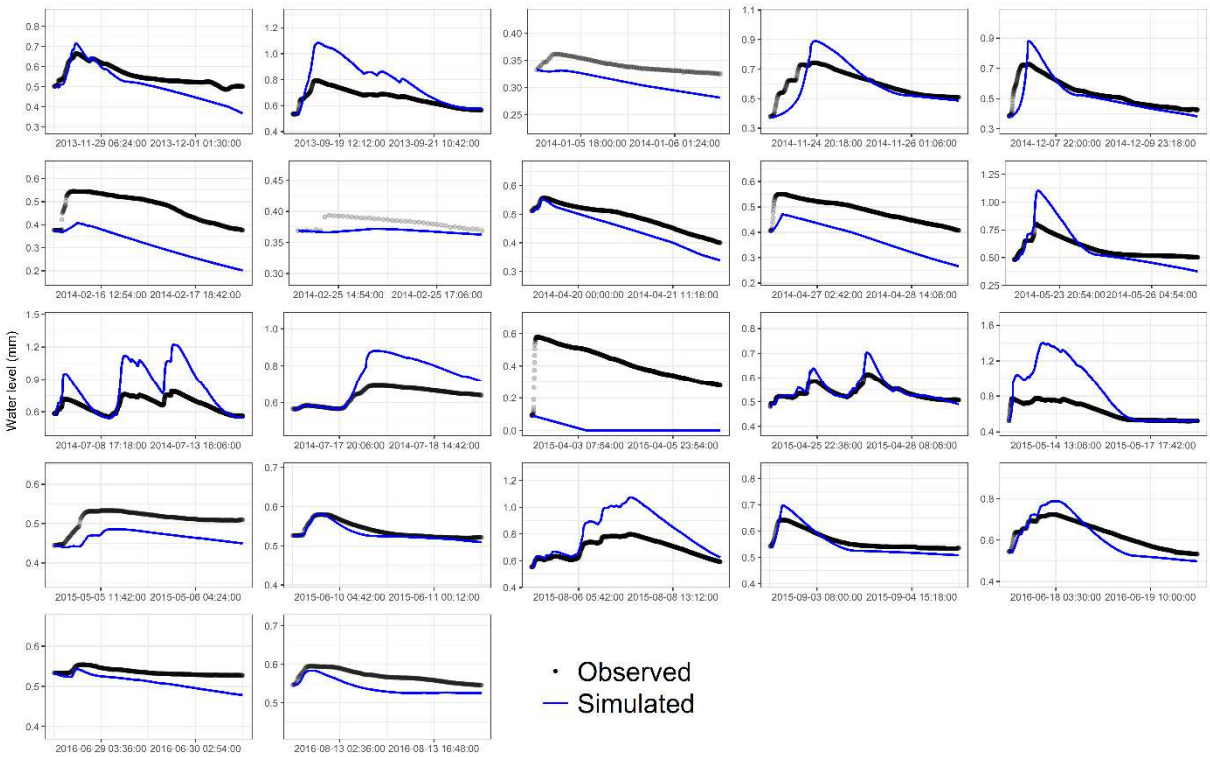


*Figure 6: Observed versus modelled water levels in the filter (black line with points = measured; blue line = simulated with the proposed model)*

*Discussion of the values of calibrated parameters*

The calibrated value of $K_s$ (5 x $10^{-4}$ m $s^{-1}$) was one order of magnitude higher than expected, the design value of the sandy layers of the basin being 6.4 x $10^{-5}$ m $s^{-1}$ (i.e., 230 mm. $h^{-1}$). This high value of the saturated hydraulic conductivity compares to typical values for sandy or gravels lithofacies (Goutaland et al., 2013). This might be due to the fact that in reality, the filter is fully vegetated with mature plants and developed root systems. The role of vegetation in increasing the hydraulic conductivity of bioretention systems is well documented and understood (Di Prima et al., 2020; Le Coustumer et al., 2009; Virahsawmy et al., 2013). The root systems, combined with bioturbation (animal and insects burrows) and even potential constructed shortcuts (the monitoring bores), can act as preferential (macropores) flow paths for water, increasing the effective hydraulic conductivity of the

387 filter. In this context, $K_s$ represents the bulk saturated hydraulic conductivity, encompassing
388 the soil matrix and the effect of macropores (Lassabatere et al., 2019).
389
390 The calibrated orifice coefficient $C_{out}$ ($2 \times 10^{-3}$) was within the order of magnitude of what
391 could have been expected, usually found in the literature for perforated PVC pipes, though
392 this value would be hard to estimate in reality. Perforated pipes have holes with a specific
393 area around 2100 $mm^2/m$ (Department of Planning and Local Government of South
394 Australia, 2010), which, for a 100 m long pipe, with a clogging factor of 0.5 and a discharge
395 coefficient of 0.61, would result in $C_{out}$ = 0.064. In reality, the contraction coefficient of a tiny
396 slot in a PVC is not well known, and might be lower than expected (corresponding to more
397 head loss resulting from more turbulence). In addition the actual state of clogging of the PVC
398 pipe was not known, particularly given the potential for plant roots to have penetrated the
399 orifices. The uncertainty around the design value for $C_{out}$ is therefore not negligible, but the
400 calibrated value seemed in line with the site features.
401
402 *Description of processes at the scale of rainfall events.*
403 In the previous paragraphs, the full capability of the model to simulate observations was
404 assessed. Modeled data analysis can be used to understand processes at the scale of rainfall
405 events. At the start of every event, when the volume of water entering the surface storage
406 was low, all the inflow volume could enter the filter media, with an infiltration rate
407 controlled by Eq. 5c. In other words, the limiting factor for water infiltration was the amount
408 of water available at surface that was not enough to supply the quasi-infinite water fluxes
409 predicted by Darcy's equation. Infinite water fluxes in relation with infinite hydraulic
410 gradients (difference final minus initial water pressure heads spanned over small depths at

411 short times) are typical of infiltration rates into soils without additional restrictions
412 (Lassabatere et al., 2009). Eq. 5c was then lower than the potential flux computed by Eq. 5a
413 (Darcy's law) and governed the quantity of infiltrated water.
414
415 Afterwards, as more water entered the filter profile, such a gradient diminished and the
416 related amount of water to be infiltrated at surface decreased. The infiltration was then
417 controlled by Darcy's law and the unsaturated hydraulic conductivity of the filter. In other
418 words, not all the volume of water available at surface could be infiltrated, and any new
419 volume of entering water might add to the remaining volume of water. As a result, the water
420 began to pond at the surface, making the water levels rise. Meanwhile, the infiltrated water
421 increased the water level in the filter up to the level required for the onset of the underdrain
422 flow (Figure 7, left panels). Even with underdrain outflow, the water level in the filter was
423 not necessarily constant, but could continue to increase right up to the top of the filter
424 surface (Figure 7). In this case, the infiltrating water flux exceeded the sum of the outflow
425 rate, evapotranspiration and exfiltration to subsoils. As time passed and the rainfall events
426 ended, the inflow fluxes began to decrease, stopped in most cases, and became lower than
427 the infiltrating fluxes, thus limiting the amount of water available at the surface for
428 infiltration. Eq. 5c became again the limiting factor for infiltration into the filter. Meanwhile,
429 the water level decreased at surface (see the tail of Figure 7, left and right panels).
430
431 For some events (Figure 7, right panels), the basin filled up, with water levels getting close to
432 the surface. Consequently, the amount of water to be infiltrated was then truncated to the
433 space available in the filter. The equation Eq 5b became the minimum among equations (5),
434 thus driving the infiltrated volume. In the case of large rainfall events, the water levels in the

filter eventually reached the surface, increasing water ponding, sometimes up to the overflow level. The system was then fully saturated. Afterwards, following the decrease in entering fluxes, the volume of water in the filter decreased by evapotranspiration, exfiltration and underdrain flow, allowing the water from the surface to infiltrate again. With the decrease of water levels in the filter, the space available in the filter was no longer limiting. The infiltration shifted back to Darcy's law. Figure 7 also illustrates the fact that the shape of modelled outflow is the same as the shape of the sum of the water levels in the filter media and at the surface. The underdrain outflow rate (Eq 8) is controlled by the orifice coefficient $C_{out}$,, which proved to drive most of the behaviour of the model of the bioretention basin. If $C_{out}$ was too high, the orifice would limit the water level in the filter, preventing it from reaching the surface, which was not consistent with some observations. Conversely, too low values of $C_{out}$ would lead to full saturation of the bio-retention system even for small rainfall amounts.

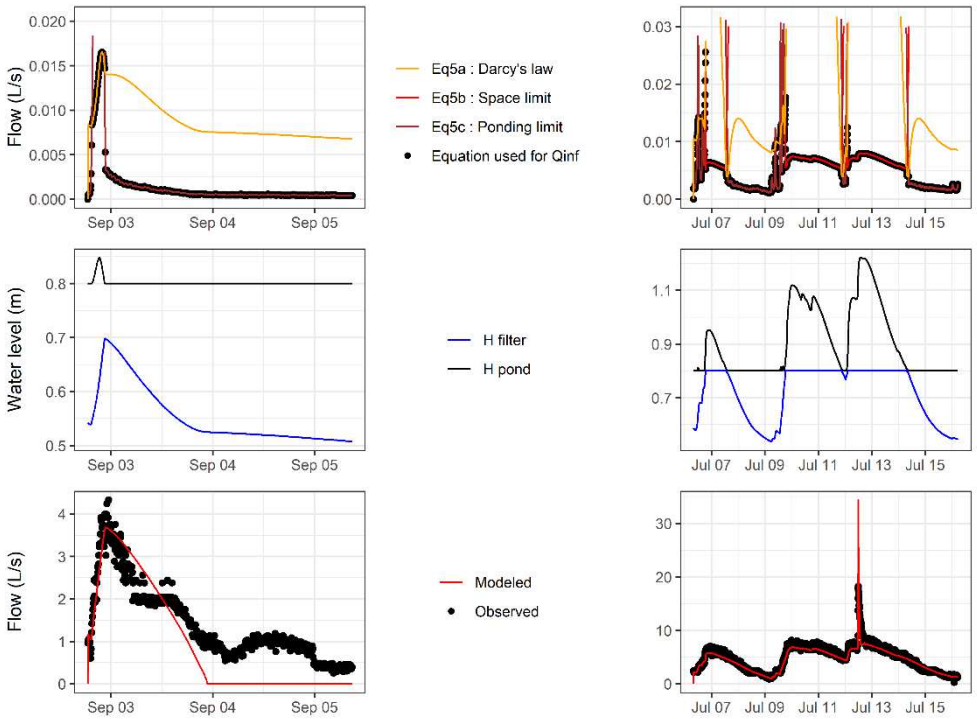

449 *Figure 7: For two rainfall events (right/left): Top: Infiltration fluxes from the surface store to*
450 *the filter media. Middle: Water levels at the surface (black line) and in the filter media (blue*
451 *line). Bottom: Modelled and observed outflows*
452

*Genericity of the proposed model, limitations and future research*

The proposed model may be applied to any bioretention system. Indeed, it requires the calibration of two key parameters to fix *a priori*: the saturated hydraulic conductivity of the filter – usually obtainable - and the coefficient $C_{out}$ that characterizes the underdrain – much harder to estimate. All the other parameters can be easily described from readily-available design information (see table 1). Most of them are standard design features of the bioretention system (area, thickness, etc.). The filter porosity, wilting point, and field capacity can be easily fixed as a function of the type of material constituting the filter, based on widely known properties. We advise keeping the specific parameters $m$ and $\tau$ to the values of 0.5, which suits an extensive range of coarse materials. The low number of parameters to calibrate reduces concerns regarding parameter equifinality and non-uniqueness (Pollacco, J.A.P. et al., 2013; Pollacco et al., 2008). These parameters should be estimated using a few rainfall events. The proposed model can be considered as a sound basis for further developments. First of all, the model focuses on the simulation of the piped outflow fluxes including the overflow and the underdrain outflow. However, modelling of water levels in the filter must be improved. The proposed model was not able to deal with empty initial conditions. For events with very little water in the filter initially, the initial effective saturation was set to the wilting point (Eq 2a), but such values were too low for the infiltration to 'start' (Eq 4 resulting in very low unsaturated hydraulic conductivity). This resulted in water staying in the ponding zone and not entering into the filter, and therefore there was no outflow modeled at all (see event of April 2015, 3$^{rd}$ row and 3$^{rd}$ column on Figures 4 and 6). Better accounting for initial conditions is necessary for future versions.

To alleviate such problems, we suggest working on the implementation the concomitant fit of water fluxes and water levels to estimate the model input parameters. Several weighing procedures could be tested to see the improvement on fits and estimates (Pollacco, J.A. et al., 2013). We also suggest working on the improvement of approximations considered for the modelling of complex processes. First of all, capillarity effects were simplified and the water retention curves were approximated to stepwise functions. Following such approximation, a bulk saturation degree was uniformized and evenly distributed along the whole filter profile. Then, the bulk hydraulic conductivity was computed from the average saturation degree using Mualem capillary models. Meanwhile, the hydraulic gradient was discretised at the scale of the filter, by dividing the difference in water pressure head by the filter depth. This process of "averaging" at the scale of the filter, considered as one "box", is far from the precise description of the downward movement of wetting fronts and infiltration processes. The loss of precision on water level due to the gain in simplicity should be investigated in more depth, using for instance numerically generated data. In addition, the model is based on the single permeability approach, whereas preferential flow may occur in reality (due to the presence of macropores). Dual porosity or dual permeability systems could thus be considered (Gerke and Van Genuchten, 1993), as is done for models of water infiltration into soils (Lassabatere et al., 2014). The implementation of dual permeability approaches for the modelling of preferential flow, as potentially induced by plant root systems, will be the subject of further studies (Asry et al., 2021).

# 4. Conclusions

A hydrologic model of a bioretention basin was built, based on equations representing all the components of the hydrological balance (water infiltration, evapotranspiration, underdrain outflow, overflow, exfiltration) in the different components of the studied basin (surface basin, filter). The main conclusions and observations, after a thorough field validation of the model, are as follows:

- It is possible to replicate outflows of a bioretention basin with a relatively simple model provided it is calibrated. Only 2 rainfall events were used for the calibration, making it suitable for a wide range of applications where resources for calibration are limited.
- The model performed well in reproducing the overall hydrological behaviours of the basin with respects to water outflows, and in particular the main features of contrasting scenarios.
- Further improved performance (such as improved replication of water level dynamics) would require additional parameters to describe the physical functioning of the basin, in terms of water transfers between the surface, the filter and the underdrain, taking into account the whole complexity of physical processes governing water infiltration into the filter. However, these parameters will degrade the model parsimony and require additional calibration effort.
- This proposed model could be readily incorporated into an LID toolbox of catchment-scale hydrological software, which are becoming increasingly used around the world.
- The model performance is particularly sensitive to one parameter, the orifice coefficient of the underdrain perforated PVC pipe, which is very hard to physically

estimate. Further research should focus on appropriate methods for characterizing this coefficient.

With the proposed approach, we provided the first step towards the design of a user-friendly model for the operation of low-impact drainage systems, leading to manage stormwater in urban areas better. The proposed model was validated against experimental data and showed promise for further development and validation on different types of stormwater control measures.

## Acknowledgements

This work was carried out in the framework of a visiting fellowship (CRCT – CNU section 60) from INSA Lyon to the University of Melbourne. The authors thank Peter Poelsma, Robert James from the University of Melbourne, along with Hervé Négro & Nicolas Invernon (Alison), Bernard Chocat for his important work in the early stages of the development of the model, Quentin Bichet, Matthieu Marin Dit Bertoud (INSA Lyon) for their help and support. The authors also benefited from ANR INFILTRON (ANR-17-CE04-0010, funded by the French National Research Agency ANR, https://infiltron.org/) and OTHU scientific and financial support. This work was also performed within the framework of the EUR H2O'Lyon (ANR-17-EURE-0018) of Université de Lyon (UdL), within the program "Investissements d'Avenir" operated by the French National Research Agency (ANR). Code and data available upon demand to the authors. The complete algorithm and computation code (R scripts) are available as Supplementary material and the dataset used is publicly shared on the platform Zenodo (http://doi.org/10.5281/zenodo.4717453).

# References


Ahmadisharaf, E., Camacho, R.A., Zhang, H.X., Hantush, M.M., Mohamoud, Y.M., 2019. Calibration and validation of watershed models and advances in uncertainty analysis in TMDL studies. Journal of Hydrologic Engineering 24(7), 03119001.

Alamdari, N., Sample, D.J., 2019. A multiobjective simulation-optimization tool for assisting in urban watershed restoration planning. Journal of Cleaner Production 213, 251-261.

Asry, A., Bonneau, J., Fernandes, G., Lipeme Kouyi, G., Chocat, B., Fletcher, T.D., Lassabatere, L., 2021. Modelling uniform and preferential flow in bioretention systems, EGU General Assembly 2021. Online.

Bear, J., 1972. Dynamics of fluids in porous media. Courier Corporation.

BoM, 2021. Climate in Victoria. Bureau of Meteorology, http://www.bom.gov.au/?ref=logo.

Bonneau, J., Fletcher, T., Lassabatère, L., Lipeme Kouyi, G., 2021. Inflows, outflows, water levels of Wicks reserve bioretention system for 22 rainfall events [Data set]. .

Bonneau, J., Fletcher, T.D., Costelloe, J.F., Poelsma, P.J., James, R.B., Burns, M.J., 2018. Where does infiltrated stormwater go? Interactions with vegetation and subsurface anthropogenic features. Journal of Hydrology 567, 121-132.

Bonneau, J., Fletcher, T.D., Costelloe, J.F., Poelsma, P.J., James, R.B., Burns, M.J., 2020. The hydrologic, water quality and flow regime performance of a bioretention basin in Melbourne, Australia. Urban Water Journal, 1-12.

Brown, R., Skaggs, R., Hunt Iii, W., 2013. Calibration and validation of DRAINMOD to model bioretention hydrology. Journal of hydrology 486, 430-442.

Burns, M.J., Fletcher, T.D., Walsh, C.J., Ladson, A.R., Hatt, B.E., 2012. Hydrologic shortcomings of conventional urban stormwater management and opportunities for reform. Landscape and Urban Planning 105(3), 230-240.

DeBusk, K.M., Hunt, W.F., Line, D.E., 2011. Bioretention Outflow: Does It Mimic Nonurban Watershed Shallow Interflow? Journal of Hydrologic Engineering 16(3), 274-279.

Department of Planning and Local Government of South Australia, 2010. Water Sensitive Urban Design Technical Manual for the Greater Adelaide Region, in: Australia, G.o.S. (Ed.) Adelaide.

Di Prima, S., Winiarski, T., Angulo-Jaramillo, R., Stewart, R.D., Castellini, M., Abou Najm, M.R., Ventrella, D., Pirastru, M., Giadrossich, F., Capello, G., 2020. Detecting infiltrated water and preferential flow pathways through time-lapse ground-penetrating radar surveys. Science of The Total Environment, 138511.

Elliott, A., Trowsdale, S., 2007. A review of models for low impact urban stormwater drainage. Environmental Modelling & Software 22(3), 394-405.

eWater, 2014. Model for urban stormwater improvement conceptualisation (MUSIC) Version 6.1, eWater, Canberra, Australia.

eWater, 2020. MUSIC.

FAWB, 2015. Adoption Guidelines for Stormwater Biofiltration Systems, Facility for Advancing Water Biofiltration. Monash University.

Fournel, J., Forquet, N., Molle, P., Grasmick, A., 2013. Modeling constructed wetlands with variably saturated vertical subsurface-flow for urban stormwater treatment. Ecological engineering 55, 1-8.

591 Francés, A., 2008. Spatio-temporal groundwater recharge assessment: a data-integration
592 and modelling approach.
593 Gerke, H.H., Van Genuchten, M.T., 1993. A dual-porosity model for simulating the
594 preferential movement of water and solutes in structured porous media. Water resources
595 research 29(2), 305-319.
596 Goutaland, D., Winiarski, T., Lassabatere, L., Dubé, J.-S., Angulo-Jaramillo, R., 2013.
597 Sedimentary and hydraulic characterization of a heterogeneous glaciofluvial deposit:
598 Application to the modeling of unsaturated flow. Engineering Geology 166, 127-139.
599 Gülbaz, S., Kazezyılmaz-Alhan, C.M., 2017. Hydrological model of LID with rainfall-watershed-
600 bioretention system. Water resources management 31(6), 1931-1946.
601 He, Z., Davis, A.P., 2011. Process modeling of storm-water flow in a bioretention cell. Journal
602 of Irrigation and Drainage Engineering 137(3), 121-131.
603 Kasmin, H., Stovin, V., Hathway, E., 2010. Towards a generic rainfall-runoff model for green
604 roofs. Water Science and Technology 62(4), 898-905.
605 Lassabatere, L., Angulo-Jaramillo, R., Soria-Ugalde, J., Šimůnek, J., Haverkamp, R., 2009.
606 Numerical evaluation of a set of analytical infiltration equations. Water Resources Research
607 45(12).
608 Lassabatere, L., Di Prima, S., Bouarafa, S., Iovino, M., Bagarello, V., Angulo-Jaramillo, R.,
609 2019. BEST-2K Method for Characterizing Dual-Permeability Unsaturated Soils with Ponded
610 and Tension Infiltrometers. Vadose Zone Journal 18(1), 1-20.
611 Lassabatere, L., Peyneau, P.-E., Yilmaz, D., Pollacco, J., Fernández-Gálvez, J., Latorre, B.,
612 Moret-Fernández, D., Di Prima, S., Rahmati, M., Stewart, R.D., 2021. Scaling procedure for
613 straightforward computation of sorptivity. Hydrology and Earth System Sciences Discussions,
614 1-33.
615 Lassabatere, L., Yilmaz, D., Peyrard, X., Peyneau, P.E., Lenoir, T., Šimůnek, J., Angulo-
616 Jaramillo, R., 2014. New analytical model for cumulative infiltration into dual-permeability
617 soils. Vadose Zone Journal 13(12).
618 Le Coustumer, S., Fletcher, T.D., Deletic, A., Barraud, S., Lewis, J.F., 2009. Hydraulic
619 performance of biofilter systems for stormwater management: Influences of design and
620 operation. Journal of Hydrology 376(1-2), 16-23.
621 Lisenbee, W., Hathaway, J., Negm, L., Youssef, M., Winston, R., 2020. Enhanced bioretention
622 cell modeling with DRAINMOD-Urban: Moving from water balances to hydrograph
623 production. Journal of Hydrology 582, 124491.
624 Liu, J., Sample, D.J., Bell, C., Guan, Y., 2014. Review and research needs of bioretention used
625 for the treatment of urban stormwater. Water 6(4), 1069-1099.
626 Moriasi, D.N., Gitau, M.W., Pai, N., Daggupati, P., 2015. Hydrologic and water quality models:
627 Performance measures and evaluation criteria. Transactions of the ASABE 58(6), 1763-1785.
628 Mourad, M., Bertrand-Krajewski, J.-L., Chebbo, G., 2005. Stormwater quality models:
629 sensitivity to calibration data. Water science and technology 52(5), 61-68.
630 Mualem, Y., 1976. A new model for predicting the hydraulic conductivity of unsaturated
631 porous media. Water resources research 12(3), 513-522.
632 Nash, J.E., Sutcliffe, J.V., 1970. River flow forecasting through conceptual models part I—A
633 discussion of principles. Journal of hydrology 10(3), 282-290.
634 Pollacco, J.A., Mohanty, B.P., Efstratiadis, A., 2013. Weighted objective function selector
635 algorithm for parameter estimation of SVAT models with remote sensing data. Water
636 Resources Research 49(10), 6959-6978.

637 Pollacco, J.A.P., Nasta, P., Soria-Ugalde, J.M., Angulo-Jaramillo, R., Lassabatere, L., Mohanty,
638 B.P., Romano, N., 2013. Reduction of feasible parameter space of the inverted soil hydraulic
639 parameter sets for Kosugi model. Soil science 178(6), 267-280.
640 Pollacco, J.A.P., Ugalde, J.M.S., Angulo-Jaramillo, R., Braud, I., Saugier, B., 2008. A Linking
641 Test to reduce the number of hydraulic parameters necessary to simulate groundwater
642 recharge in unsaturated soils. Advances in water resources 31(2), 355-369.
643 Richards, L.A., 1931. Capillary conduction of liquids through porous mediums. physics 1(5),
644 318-333.
645 Rossman, L.A., 2010. Modeling Low Impact Development Alternatives with SWMM. Journal
646 of Water Management Modeling.
647 Rossman, L.A., 2010. Storm water management model user's manual, version 5.0. National
648 Risk Management Research Laboratory, Office of Research and ….
649 Roy-Poirier, A., Champagne, P., Filion, Y., 2010. Review of bioretention system research and
650 design: past, present, and future. Journal of Environmental Engineering 136(9), 878-889.
651 SILO, 2020. SILO climate database. data.qld.gov.au, http://data.qld.gov.au/dataset/silo-
652 climate-database, https://researchdata.edu.au/silo-climate-database.
653 Skaggs, R., 1980. DRAINMOD reference report. Methods for design and evaluation of
654 drainage-water management systems for soils with high water tables. USDASCS, South
655 National Technical Center, Fort Worth, Texas, 329.
656 Skaggs, R., 1985. Drainmod: Reference Report; Methods for Design and Evaluation of
657 Drainage-Water Management Systems for Soils with High Water Tables.
658 Van der Lee, J., Gehrels, J., 1990. Modelling aquifer recharge–introduction to the lumped
659 parameter model EARTH. Free University of Amsterdam, The Netherlands.
660 van Genuchten, M.T., 1980. A closed-form equation for predicting the hydraulic conductivity
661 of unsaturated soils 1. Soil science society of America journal 44(5), 892-898.
662 Virahsawmy, H., Stewardson, M., Vietz, G., Fletcher, T.D., 2013. Factors that affect the
663 hydraulic performance of raingardens: Implications for design and maintenance. Water
664 Science and Technology doi:10.2166/wst.2013.809 (published online 26 December 2013).
665 Walsh, C.J., Fletcher, T.D., Burns, M.J., 2012. Urban Stormwater Runoff: A New Class of
666 Environmental Flow Problem. PLoS ONE 7(9), e45814.
667